Research on Design and Experiment of a Wearable Hand Rehabilitation Device Driven by Fiber-Reinforced Soft Actuator *

Kaiwei Ma, Zhenjiang Jiang, Shuang Gao, Guo-Ping Jiang, *Senior Member*, *IEEE*, and Fengyu Xu

***Abstract*— Fiber-reinforced soft actuators have great potential for the development of wearable technology. However, its complex structural design, nonlinear soft material body, fluid-driven dynamics and high manufacturing costs have brought huge challenges to system modeling, control and application. To improve this situation, a novel fiber-reinforced soft actuator is designed and analyzed. First, a wearable hand rehabilitation device based on fiber-reinforced soft actuators with three-air-chamber structure is designed. Next, using Yeoh model and principle of virtual work, we establish a bending mathematical model of the soft actuator, whose input parameters are air pressure P and winding number N, and output parameter is bending angle β. Finally, through the finite element analysis, the optimal N is obtained, and the correctness of the model is verified. To verify the above research, an experimental platform is constructed. The results show that the relative error of the model is in an acceptable state. The device can imitate common gestures, easily grasp objects with a volume of 1.6 dm^3 and mass of 335.7 g, which can realize the hand rehabilitation training.**

I. Introduction

Partial or complete loss of hand function is the most common symptom after cerebral apoplexy, muscular dystrophy and incomplete spinal cord injury [1]–[3]. People with this disorder will lose the ability to accurately control their hands and fingers, as well as the ability to carry out daily activities. For such patients, physical treatment such as grasping is required in addition to recovery treatment of drugs [4], [5]. Therefore, wearable hand rehabilitation device has become an important medical equipment for patients with hand dysfunction to carry out specific rehabilitation training or daily activities.

In recent years, many scholars and experts have conducted in-depth research on its structure and control. They put forward many types of hand rehabilitation devices, such as jointless tendon-driven [6], exoskeleton linkage structure [7]–[9], cable driven [10], [11] and master-slave control mode [12], [13]. These rigid devices have the characteristics of high control precision, multiple rehabilitation functions, high price and strong professionalism. Therefore, it is mainly used in clinical treatment environment. Due to the use of hard materials, the patient feels less comfortable during the treatment. Moreover, improper operation is likely to cause secondary injuries such as finger bending or twisting. More importantly, hand rehabilitation is a lengthy process, and patients prefer to do it at home.

Therefore, in order to avoid the above problems, researchers began to use soft actuators to design hand rehabilitation device, hoping to achieve good fit, simple production, low price, and suitable for family rehabilitation treatment [14]–[16]. These used soft actuators can be divided into non-fiber-reinforced soft actuators, and fiber-reinforced soft actuators. After years of research, the former can be subdivided into: hydraulic/pneumatic actuator [17], [18], tendon-driven actuator [19], fabric-based actuator [20], [21], segmented PneuNets bending actuator [22], and soft-elastic composite actuator [23]. The latter mainly focuses on the design of its structure and control method. Wirekoh et al. [24] proposed fiber-reinforced bending pneumatic artificial muscle with a collapsed zero-volume air chamber. Chatterjee et al. [25] studied the effect of fiber orientations on the large deformation mechanics of fiber-reinforced soft actuator. Chen et al. [26] used two high-speed on/off valves to realize the control of the actuator. Bruder et al. [27] explored a novel methodology to represent and calculate the generalized forces generated by the internal pressure.

In summary, non-fiber-reinforced soft actuator hand rehabilitation devices generally have problems such as complex structure, poor air tightness and small contact force, while fiber-reinforced soft actuator hand rehabilitation devices have simple structure and can provide large bending angle. At present, there are relatively few studies on fiber-reinforced soft actuator hand rehabilitation devices. Moreover, most of them are based on experiments. There is little theoretical modeling and analysis of their deformation.

To address these shortcomings, a novel fiber-reinforced soft actuator for wearable rehabilitation device is designed in this article. The actuator can bend in any direction and angle by controlling the air pressure in the three-air-chamber structure. The bending deformation mechanism of the actuator is analyzed, and a mathematical model is established. The experiment of the physical model shows that the finger bending angle, grasping force and grasping volume of the device can meet the requirements of hand rehabilitation training in daily life.

*This work was supported in part by the Major Natural Science Research Project of Colleges and Universities in Jiangsu Province under Grant 21KJA460013, in prat by the Natural Science Foundation of Jiangsu Province under Grant BK20201379, in part by the Fundamental Research Funds for the Central Universities under Grant MCCSE2021A02, in part by the Natural Science Research Start-up Foundation of Recruiting Talents of Nanjing University of Posts and Telecommunications under Grant NY220140, and in part by Innovation and Entrepreneurship Program of Jiangsu Province under Grant JSSCBS20210523. *(Corresponding author: Fengyu Xu.)*

The authors are with the College of Automation & College of Artificial Intelligence, Nanjing University of Posts and Telecommunications, Nanjing 210023, China, and also with the Key Laboratory of Measurement and Control of Complex Systems of Engineering, Ministry of Education, Southeast University, Nanjing 210096, China makaiwei@live.com; 1693946558@qq.com; 1925938770@qq.com; jianggp@njupt.edu.cn; xufengyu598@163.com

II. Design of Hand Rehabilitation Device

To meet the needs of hand rehabilitation, it is necessary to study the motion range of finger joint to determine the design parameters. Here, the functional range of motion of the hand joints is selected [28], [29].

A. Structural Design

According to the analysis of human hand biological structure, a wearable hand rehabilitation device is designed, as shown in Fig. 1. The device is composed of five fiber-reinforced soft actuators and a bionic bottom plate.

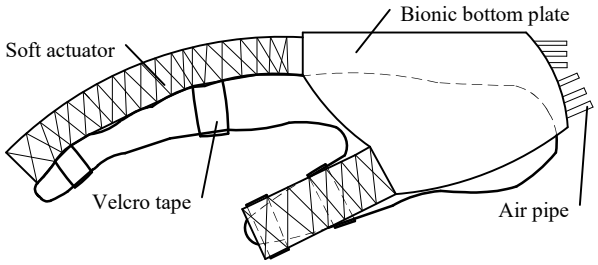

Fig. 1. Schematic diagram of wearable hand rehabilitation device based on fiber-reinforced soft actuator.

Theoretically, 5 different actuators need to be designed for the device. However, the index finger and ring finger are close in global functional range of motion [29]. Moreover, they are very close in length. Therefore, it can be reduced to 4 groups — thumb, index (ring) finger, middle finger, and little finger.

B. Design of Soft Actuator

Soft actuator is an important part of the wearable hand rehabilitation device. Its structural design directly affects the performance of the device. So, we design a three-air-chamber structure in the actuator. A fiber reinforced layer contained in the outer surface, which is consists of a double helix structure of Kevlar fiber. Its structure is shown Fig. 2.

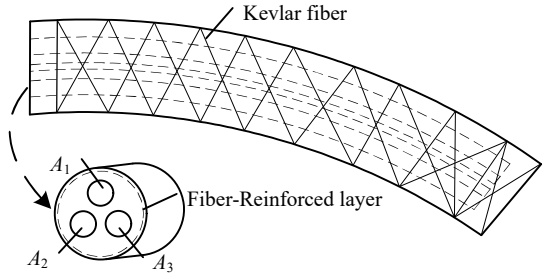

Fig. 2. Schematic diagram of soft actuator with fiber-reinforced layer.

In the figure, A_1, A_2, A_3 represent 3 air chambers, which can be inflated respectively through the air pipe to realize the independent bending movement. During the process, the fiber layer limits the radial expansion of the air chamber. Therefore, the main deformation mode of the air chamber is axial elongation. For this actuator, the winding number of Kevlar fiber is an important factor affecting the bending performance of the soft actuator, which is the focus of this letter. Other parameters are secondary factors. Therefore, these parameters are set as fixed values, as shown in Table I. The actual measured value is used for the finger length. Other parameters mainly refer to the silicone rubber processing technology and the structural design scheme of soft actuator.

TABLE I
Sturcture Parameters of Soft Actuators

Item	Value
Length of fingers[1]	90, 100, 110, 120 mm
Air chamber length of each finger[1]	80, 90, 100, 110 mm
Diameter of soft actuators	24 mm
Diameter of air chamber	4 mm
Included angle of each air chamber	120°
Diameter of fiber layer	20 mm
Diameter of Kevlar fiber	0.4 mm

[1] From short to long: thumb, little finger, index (ring) finger, middle finger.

III. Mathematical Modeling of Soft Actuator

The operation of wearable hand rehabilitation device is based on the orderly operation of soft actuator. Therefore, it is necessary to establish the theoretical model of its bending deformation.

A. Establishment of Strain Energy Density Function

The soft actuator is made of silicone rubber, which is a typical polymer nonlinear hyper-elastic material. At present, the mechanical properties of the material are analyzed by establishing strain energy density function [**?**]. Therefore, Yeoh model is selected to establish the strain energy density function W of the actuator:

$$W = C_{10}(I_1 - 3) + C_{20}(I_1 - 3)^2 \tag{1}$$

whose I_1 is

$$I_1 = \lambda_1^2 + \lambda_2^2 + \lambda_3^2 \tag{2}$$

where C_{10} and C_{20} are constant coefficients of silicone rubber material, which are obtained by tensile experiment and data fitting. I_1 is the first invariant of the stress tensor. λ_1, λ_2 and λ_3 are the principal tensile ratios in axial, radial and circumferential directions, respectively.

When an air chamber is filled with compressed air, the deformation is shown in Fig. 3. By comparing the initial shape and bending shape of the soft actuator, the principal tensile ratios can be computed as

$$\begin{cases} \lambda_1 = l/l_0 \\ \lambda_2 = r/r_0 \\ \lambda_3 = \left(t_1/t_{10} + t_2/t_{20} + t_3/t_{30} + t_4/t_{40}\right)/4 \end{cases} \tag{3}$$

where l_0 and r_0 are the length and radius of the central axis of the air chamber before deformation, respectively. t_{10}, t_{20}, t_{30} and t_{40} represent the wall thickness of the air chamber

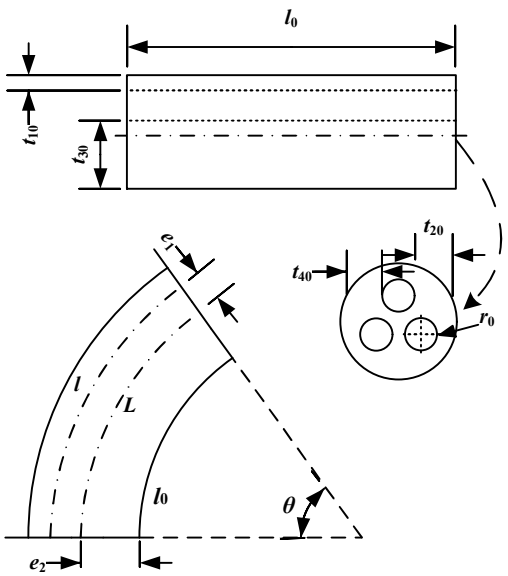

Fig. 3. Schematic diagram of structural change of the single air chamber inflation of soft actuator.

before deformation, respectively. l, r, t_1, t_2, t_3 and t_4 are the parameters corresponding to l_0, r_0 t_{10}, t_{20}, t_{30} and t_{40} after bending, respectively.

B. Bending Model of Single Air Chamber

The designed soft actuator consists of a uniformly distributed three-air-chamber structure and a fiber reinforced layer. When an air chamber is inflated, it is assumed that the actuator bends with constant curvature in the plane. According to the geometric relationship, we have

$$\begin{cases} L = l_0 + e_2\theta \\ l = l_0 + (e_1 + e_2)\,\theta \end{cases} \tag{4}$$

$$\begin{cases} t_1 = R - e_1 - r \\ t_2 = \sqrt{R^2 - e_1^2} - r \\ t_3 = R + e_1 - r \\ t_4 = \sqrt{R^2 - e_1^2} - r \end{cases} \tag{5}$$

where L is the length of the actuator central axis. θ is the bending deformation center angle of the actuator under single air chamber inflation. e_1 is the distance from the central axis of the air chamber to the central axis of the actuator. e_2 is the distance between the central axis of the actuator and the non-extensible surface. R is the radius of the actuator section after bending.

Assuming that the fibers are evenly wound and not extensible, we have

$$B^2 = l_0^2 + (2\pi RN)^2 \tag{6}$$

where B is the length of a single fiber line. N is the winding number of the Kevlar fiber in fiber-reinforced layer.

When a single air chamber is filled with compressed air, the volume change of each part of the actuator is

$$V_a = \pi r^2 l \tag{7}$$

$$V_r = \pi R^2 L - \pi r^2 l - 2\pi r_0^2 l_0 \tag{8}$$

$$V_{r,0} = \pi\left(R_0^2 - r_0^2\right) l_0 - 2\pi r_0^2 l_0 \tag{9}$$

where V_a represents the volume of compressed air inside the air chamber. V_r ($V_{r,0}$) represents the volume of silicone rubber after (before) bending.

Due to the incompressibility of the material, the volume of silicone rubber remains unchanged during deformation. So, $V_r = V_{r,0}$. Substituting (4), (6), (8), (9) into this equation, we have

$$r = \sqrt{\frac{R^2\left(l_0 + e_2\theta\right) - \left(R_0^2 - r_0^2\right) l_0}{l_0 + (e_1 + e_2)\,\theta}} \tag{10}$$

with

$$R = \frac{\sqrt{B^2 - \left(l_0 + e_2\theta\right)^2}}{2\pi N} \tag{11}$$

Because there is no external force, the bending deformation of the soft actuator comes entirely from the work done by the air pressure P. According to the principle of virtual work

$$P\frac{dV_a}{d\theta} + V_r\frac{dW}{d\theta} = 0 \tag{12}$$

Substituting (4), (7), (8) into (12), we can get

$$P = -\frac{\left(R_0^2 - r_0^2\right) l_0 dW/d\theta}{2\left[l_0 + (e_1 + e_2)\,\theta\right] r dr/d\theta + r^2\left(e_1 + e_2\right)} \tag{13}$$

where $dW/d\theta$, $dr/d\theta$ can be written as functions containing θ and N using (1) $\sim$ (3), (5), (10), (11).

So, for a single air chamber i, the relationship among the bending deformation center angle θ_i, the air pressure P_i and the winding number N is

$$\theta_i = f\left(P_i, N\right), \quad i = 1, 2, 3 \tag{14}$$

C. Theoretical Model of Soft Actuator Bending Deformation

The final shape of the actuator is formed by the coupling of air pressure in each air chamber. Therefore, it is necessary to use the single air chamber bending deformation theory to establish the relationship among bending angle β, air pressure P_i and coil turns N, and bending deformation center angle θ_i.

Fig. 4 describes the bending of the actuator under the combined action of three air chambers. The deflection angle is the angle φ between the bending direction and the initial x-axis. It is assumed that the bending curvature of each air

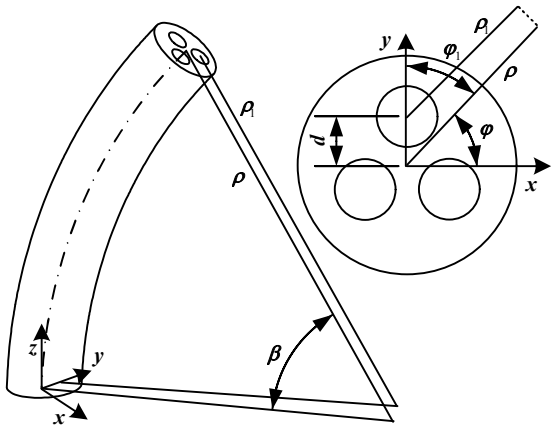

Fig. 4. Bending diagram of soft actuator under multi-air-chamber inflation.

chamber is the same. The curvature radius of the central axis in the bending is ρ.

The curvature radius of each air chamber is

$$\rho_i = \rho - d\cos\varphi_i \tag{15}$$

where ρ_i and φ_i represent the radius of curvature and deflection angle corresponding to air chamber i, respectively. d is the distance from the central axis of the actuator to the central axis of the air chamber.

Multiply both sides of (15) by β, we can get

$$l = l_i + \beta d\cos\varphi_i \tag{16}$$

where

$$l_i = l_0 + (e_1 + e_2)\,\theta_i \tag{17}$$

According to the geometry of the three air chambers, φ_i can be written as

$$\varphi_1 = 90 - \varphi,\ \varphi_2 = 210 - \varphi,\ \varphi_3 = 330 - \varphi \tag{18}$$

It is assumed that the length of each axis satisfies the following relationship

$$l = \frac{l_1 + l_2 + l_3}{3} \tag{19}$$

Combining (16) $\sim$ (19), we have

$$\varphi = \arctan\frac{l_2 + l_3 - 2l_1}{\sqrt{3}(l_2 - l_3)} \tag{20}$$

Then, according to the geometric relationship, the bending angle β can be expressed by the following equation:

$$\beta = \frac{2\sqrt{l_1^2 + l_2^2 + l_3^2 - l_1 l_2 - l_1 l_3 - l_2 l_3}}{3d} \tag{21}$$

where l_1, l_2, l_3 can be written as funcitons containing θ_i, P_i and N using (14) and (17).

Therefore, the bending angle β can be rewritten as

$$\beta = f(P_i, N) \tag{22}$$

Through the above process, the mathematical model of soft actuator is obtained, which lays the foundation for the theoretical analysis of bending angle and the continuous control of the soft actuator.

IV. Finite Element Analysis of Soft Actuator

Here, the soft actuator corresponding to the index (ring) finger is selected as the simulation object. The grasping process, that is, the two air chambers are filled with the same air source, is selected as the simulation condition.

A. Analysis of Winding Number

Under the same condition, different winding numbers ($N = 0, 10, 20, 30, 40, 50, 60$) are selected to realize the $\beta = 90^\circ$ of the actuator. Therefore, seven different finite element analysis modules need to be analyzed, and the results are shown in Fig. 5.

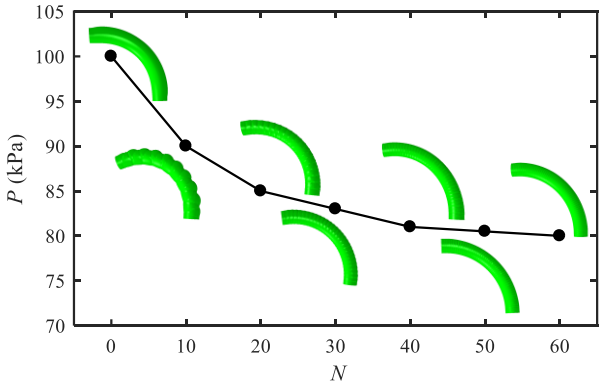

Fig. 5. Relationship between air pressure P and winding number N of Kevlar fiber.

As seen from Fig. 5, the fiber-reinforced layer with high turns ($10 \le N \le 50$) can effectively inhibit the radial expansion of pneumatic structure. When $N > 50$, the inhibition effect of radial expansion, and the change of air pressure become no longer obvious. Therefore, $N = 50$ can be selected.

At the same time, it can be seen that compared with the pneumatic soft actuator without fiber-reinforced layer, the actuator with fiber-reinforced layer needs less input air pressure to reach the same bending angle. In other words, the fiber reinforced layer can significantly improve the bending efficiency of pneumatic structure.

B. Bending Performance Simulation of Soft Actuator

After N is determined, the air chambers are filled with the same air pressures ($P =$ 10, 20, 30, 40, 50, 60, 70, 80, 90 kPa) in turn to obtain the simulated bending angle β_s. Then, the corresponding theoretical bending β_t is obtained by using the (22). Record and calculate the relative error with $\Delta = |\beta_t - \beta_s| / \beta_s \times 100\%$. The results are shown in Fig. 6.

It can be seen that the relative errors are less than 14%, which verifies the correctness of the theoretical model.

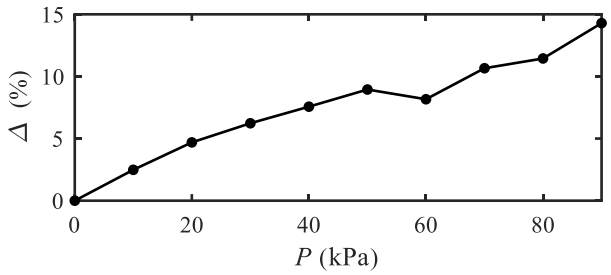

Fig. 6. Relative error between theoretical value and simulation value of bending angle.

Because many assumptions are used in the mathematical model, the relative increases with the increase of air pressure. When $P > 60$ kPa, the relative error exceeds 10%, so the recommended working air pressure is within 60 kPa.

The result of finite element analysis is ideal and can be set as an accurate value. Thus, Fig. 6 shows that the maximum modeling error of (22) under the recommended working pressure is 8.9%, which is mainly caused by approximations and assumptions in the modeling process.

V. Experiment

The device (including the soft actuators) is manufactured by 3D printing, silicone rubber, Kevlar fiber and air pipe. Then we need to use experiments to verify the above contents.

A. Construction of Experimental Platform

The experimental platform is shown in Fig. 7. In the experiment, the bending angle can be obtained from the coordinate paper. The fingertip force can be detected by the pressure sensor. The experiments of soft actuators are divided into 4 groups according to Table I.

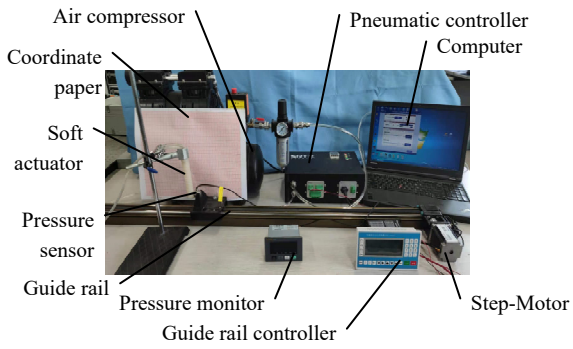

Fig. 7. Photograph of experimental setup.

B. Bending Angle Test

To verify the correctness of the theoretical model, the bending angle β_f of the soft actuator corresponding to each finger needs to be tested. This requires fixing the end of the soft actuator so that the whole finger is perpendicular to the ground. Then, the test is carried out using the air pressures and conditions in Subsection IV-B. After the deformation of the tested finger is stable, record its bending angle with coordinate paper. Take the average value after 5 measurements, and the results are shown in Fig. 8(a).

It can be seen that the activity ranges of thumb, index (ring) finger, middle finger and little finger are $0 \sim 97.7°$, $0 \sim 129.1°$, $0 \sim 157.4°$, and $0 \sim 115.5°$, respectively, which basically meet the requirements of daily functional movement of hand. And there is a significant positive correlation between the bending angle and the finger length under the same air pressure.

Define the error $\Delta\beta = \beta_f - \beta_t$. Then, the error curve of the bending angle of each finger is obtained, as illustrated in Fig. 8(c).

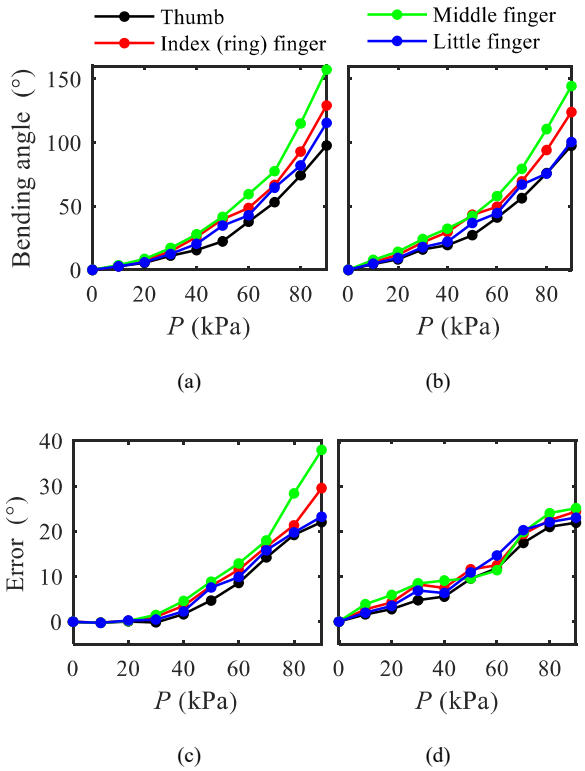

Fig. 8. Results and analysis of bending angle test. (a) Test value of unidirectional bending angle of each finger without a human hand. (b) Test value of unidirectional bending angle of each finger with a human hand. (c) Error diagram between test value and theoretical value without a human hand. (d) Error diagram between test value and theoretical value with a human hand.

In general, the measured bending angle of each finger is significantly greater than the theoretical value. From the curve trend, it can be seen that the error of each finger increases with the increase of air pressure. Moreover, when $P \leq 30$ kPa, the relative error of the bending angle of each finger is less than 8%, which is in an ideal state. This indicates that the theoretical model is correct. When $30 < P \leq 60$ kPa, the relative error is less than 29%, which is in an acceptable state. When $P > 60$ kPa, the relative error of the theoretical model is up to 36%, which is in a non-ideal state. The main reason for these phenomena

is that the theoretical model adopts more assumptions, the manufacturing process has larger errors, and the physical model shows higher nonlinear characteristics under larger strain.

A subject puts on the device and repeats the test with his fingers relaxed. At this time, the overall range of motion β_h (shown in Fig. 8(b)) can be obtained. Define the error $\Delta\beta_h = \beta_h - \beta_t$, the corresponding error curve is shown in Fig. 8(d).

Under the same air pressure, for most test points, $\beta_h < \beta_f$, $\Delta\beta_h < \Delta\beta$, and $\Delta\beta_h$ has obvious randomness. This indicates that the addition of the hand significantly reduces the range of motion of the soft actuator. The coupling between hand and equipment adds uncertainty to this phenomenon.

C. Comprehensive Performance Test

According to the above mathematical modeling, finite element simulation analysis and experimental results, the comprehensive performance test of wearable hand rehabilitation device based on soft actuators can be carried out. The main application scenarios of typical hand rehabilitation training are analyzed, and the test is divided into gesture experiment and grasping experiment. To show the results objectively, the experiments adopt the mode without hands.

Fig. 9 shows the results of the gesture experiment. It can be seen that the device has a high degree of flexibility and can better simulate the gestures used in daily life.

(a) (b) (c)

Fig. 9. Gesture experiment of rehabilitation device under no-load state. (a) Victory. (b) OK. (c) Three.

At the same time, use the daily necessities in Table II to test the device, and the results are shown in Fig. 10. The device can adapt to objects of different sizes and shapes and easily grab fragile items, which displays good flexibility, adaptability and surface adhesion. With a maximum grasping force of 3.3 N, the device can become an ideal equipment for hand rehabilitation training.

Through the above tests, we can find that compared with the rigid device [13], the fingers of the soft device show infinite degrees of freedom. Compared with other soft actuators [17], [18], the device can achieve highly controllable continuous deformation due to the theoretical model of bending deformation. At the same time, due to the unique three-air-chamber structure, the soft actuator can realize bending in any direction.

TABLE II
EXPERIMENTAL DAILY NECESSITIES AND RELATED PARAMETERS

Item	Shape	Volume (dm^3)	Mass (g)
Beverage bottle	Cylinder	1.6	335.7
Orange	Sphere	1.1	128.6
Glass cup	Cylinder	1.0	159.9
Bananas	Irregular	1.5	320.0
Milk box	Cube	0.25	269.3
Spray bottle	Cone	1.4	61.1

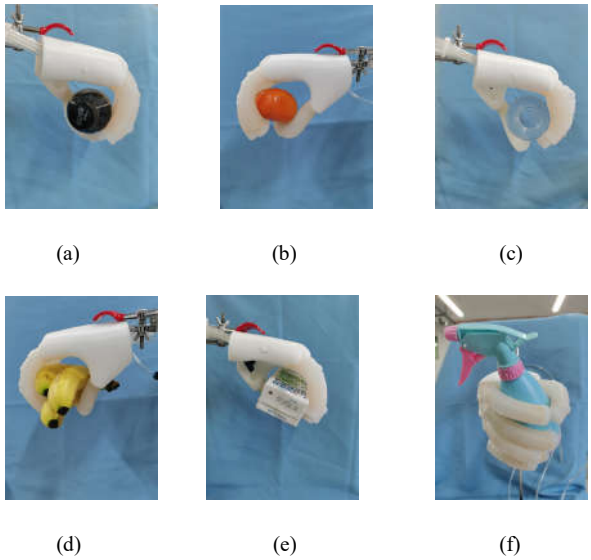

(a) (b) (c)

(d) (e) (f)

Fig. 10. Grasping experiment of rehabilitation device. (a) Beverage bottle. (b) Orange. (c) Glass cup. (d) Bananas. (e) Milk box. (d) Spray bottle.

VI. CONCLUSION

In this article, a fiber-reinforced soft actuator was designed and analyzed for the wearable hand rehabilitation device. Using Yeoh model and structural analysis, the mathematical model of bending deformation of soft actuator was established. Before solving the model, the winding number of fiber-reinforced layer needed to be determined by finite element simulation analysis. After that, the bending angle corresponding to different air pressure and air chamber inflation mode could be obtained by numerical calculation of the model.

To validate the proposed soft actuator, a hand rehabilitation device test platform was constructed. The results indicated that the bending angle of the soft actuator could satisfy the daily motion range of each finger. Under the working air pressure, the relative error of bending angle could be less than 29%. In the handless mode, the device could imitate a variety of gestures and grasp various objects, which could meet the daily hand rehabilitation training.

REFERENCES

[1] J. Weichbrodt, B.-M. Eriksson, and A.-K. Kroksmark, "Evaluation of hand orthoses in duchenne muscular dystrophy," *Disabil. Rehabil.*, vol. 40, no. 23, pp. 2824–2832, 2018.

[2] B. K. Pedersen and B. Saltin, "Exercise as medicine evidence for prescribing exercise as therapy in 26 different chronic diseases," *Scand. J. Med. Sci. Sports*, vol. 25, no. S3, pp. 1–72, 2015.

[3] G. E. Francisco, N. Yozbatiran, J. Berliner, M. K. O'Malley, A. U. Pehlivan, Z. Kadivar, K. Fitle, and C. Boake, "Robot-assisted training of arm and hand movement shows functional improvements for incomplete cervical spinal cord injury," *Am. J. Phys. Med. Rehabil.*, vol. 96, no. 10, pp. S171–S177, 2017.

[4] M. Bobin, M. Anastassova, M. Boukallel, and M. Ammi, "Design and study of a smart cup for monitoring the arm and hand activity of stroke patients," *IEEE J. Transl. Eng. Health Med.-JTEHM*, vol. 6, pp. 1–12, 2018.

[5] C. G. Rose and M. K. OMalley, "Hybrid rigid-soft hand exoskeleton to assist functional dexterity," *IEEE Robot. Autom. Lett.*, vol. 4, no. 1, pp. 73–80, 2019.

[6] J. Yang, H. Xie, and J. Shi, "A novel motion-coupling design for a jointless tendon-driven finger exoskeleton for rehabilitation," *Mech. Mach. Theory*, vol. 99, pp. 83–102, 2016.

[7] I. Jo and J. Bae, "Design and control of a wearable and force-controllable hand exoskeleton system," *Mechatronics*, vol. 41, pp. 90–101, 2017.

[8] D. Wang, Q. Meng, Q. Meng, X. Li, and H. Yu, "Design and development of a portable exoskeleton for hand rehabilitation," *IEEE Trans. Neural Syst. Rehabil. Eng.*, vol. 26, no. 12, pp. 2376–2386, 2018.

[9] J. A. Dez, A. Blanco, J. M. Cataln, F. J. Badesa, L. D. Lled, and N. Garca-Aracil, "Hand exoskeleton for rehabilitation therapies with integrated optical force sensor," *Adv. Mech. Eng.*, vol. 10, no. 2, pp. 1–11, 2018.

[10] F. Aggogeri, T. Mikolajczyk, and J. OKane, "Robotics for rehabilitation of hand movement in stroke survivors," *Adv. Mech. Eng.*, vol. 11, no. 4, pp. 1–14, 2019.

[11] K. Serbest, M. Kutlu, O. Eldogan, and I. Tekeoglu, "Development and control of a home-based training device for hand rehabilitation with a spring and cable driven mechanism," *Biomed. Eng.-Biomed. Tech.*, p. 000010151520190267, 2021. [Online]. Available: https://doi.org/10.1515/bmt-2019-0267

[12] S. Ueki, H. Kawasaki, S. Ito, Y. Nishimoto, M. Abe, T. Aoki, Y. Ishigure, T. Ojika, and T. Mouri, "Development of a hand-assist robot with multi-degrees-of-freedom for rehabilitation therapy," *IEEE-ASME Trans. Mechatron.*, vol. 17, no. 1, pp. 136–146, 2012.

[13] M. Cortese, M. Cempini, P. R. de Almeida Ribeiro, S. R. Soekadar, M. C. Carrozza, and N. Vitiello, "A mechatronic system for robot-mediated hand telerehabilitation," *IEEE-ASME Trans. Mechatron.*, vol. 20, no. 4, pp. 1753–1764, Aug 2015.

[14] A. Moss, M. Krieg, and K. Mohseni, "Modeling and characterizing a fiber-reinforced dielectric elastomer tension actuator," *IEEE Robot. Autom. Lett.*, vol. 6, no. 2, pp. 1264–1271, 2021.

[15] K. Shiota, S. Kokubu, T. V. Tarvainen, M. Sekine, K. Kita, S. Y. Huang, and W. Yu, "Enhanced kapandji test evaluation of a soft robotic thumb rehabilitation device by developing a fiber-reinforced elastomer-actuator based 5-digit assist system," *Robot. Auton. Syst.*, vol. 111, pp. 20–30, 2019.

[16] F. Xu, J. Quansheng, Y. Lu, and G. Jiang, "Modelling of a soft multi-chambered climbing robot and experiments," *Smart Mater. Struct.*, vol. 30, no. 3, p. 035009, feb 2021. [Online]. Available: https://dx.doi.org/10.1088/1361-665X/abd910

[17] H. K. Yap, N. Kamaldin, J. H. Lim, F. A. Nasrallah, J. C. H. Goh, and C.-H. Yeow, "A magnetic resonance compatible soft wearable robotic glove for hand rehabilitation and brain imaging," *IEEE Trans. Neural Syst. Rehabil. Eng.*, vol. 25, no. 6, pp. 782–793, June 2017.

[18] H. K. Yap, P. M. Khin, T. H. Koh, Y. Sun, X. Liang, J. H. Lim, and C.-H. Yeow, "A fully fabric-based bidirectional soft robotic glove for assistance and rehabilitation of hand impaired patients," *IEEE Robot. Autom. Lett.*, vol. 2, no. 3, pp. 1383–1390, July 2017.

[19] X. Chen, L. Gong, L. Wei, S.-C. Yeh, L. Da Xu, L. Zheng, and Z. Zou, "A wearable hand rehabilitation system with soft gloves," *IEEE Trans. Ind. Inform.*, vol. 17, no. 2, pp. 943–952, Feb 2021.

[20] L. Ge, F. Chen, D. Wang, Y. Zhang, D. Han, T. Wang, and G. Gu, "Design, modeling, and evaluation of fabric-based pneumatic actuators for soft wearable assistive gloves," *Soft Robot.*, vol. 7, no. 5, pp. 583–596, 2020, pMID: 31995436.

[21] L. Cappello, K. C. Galloway, S. Sanan, D. A. Wagner, R. Granberry, S. Engelhardt, F. L. Haufe, J. D. Peisner, and C. J. Walsh, "Exploiting textile mechanical anisotropy for fabric-based pneumatic actuators," *Soft Robot.*, vol. 5, no. 5, pp. 662–674, 2018, pMID: 30024312.

[22] J. Wang, Y. Fei, and W. Pang, "Design, modeling, and testing of a soft pneumatic glove with segmented pneunets bending actuators," *IEEE-ASME Trans. Mechatron.*, vol. 24, no. 3, pp. 990–1001, June 2019.

[23] K. H. Heung, R. K. Tong, A. T. Lau, and Z. Li, "Robotic glove with soft-elastic composite actuators for assisting activities of daily living," *Soft Robot.*, vol. 6, no. 2, pp. 289–304, 2019, pMID: 30874489.

[24] J. Wirekoh, N. Parody, C. N. Riviere, and Y.-L. Park, "Design of fiber-reinforced soft bending pneumatic artificial muscles for wearable tremor suppression devices," *Smart Mater. Struct.*, vol. 30, no. 1, p. 015013, dec 2020.

[25] A. Chatterjee, N. R. Chahare, P. Kondaiah, and N. Gundiah, "Role of fiber orientations in the mechanics of bioinspired fiber-reinforced elastomers," *Soft Robot.*, vol. 0, no. 0, p. null, 0, pMID: 33170097.

[26] C. Chen, W. Tang, Y. Hu, Y. Lin, and J. Zou, "Fiber-reinforced soft bending actuator control utilizing on/off valves," *IEEE Robot. Autom. Lett.*, vol. 5, no. 4, pp. 6732–6739, Oct 2020.

[27] D. Bruder, A. Sedal, R. Vasudevan, and C. D. Remy, "Force generation by parallel combinations of fiber-reinforced fluid-driven actuators," *IEEE Robot. Autom. Lett.*, vol. 3, no. 4, pp. 3999–4006, Oct 2018.

[28] G. I. Bain, N. Polites, B. G. Higgs, R. J. Heptinstall, and A. M. McGrath, "The functional range of motion of the finger joints," *J. Hand Surg.-Eur. Vol.*, vol. 40, no. 4, pp. 406–411, 2015, pMID: 24859993.

[29] V. Gracia-Ibez, M. Vergara, J. L. Sancho-Bru, M. C. Mora, and C. Piqueras, "Functional range of motion of the hand joints in activities of the international classification of functioning, disability and health," *J. Hand Ther.*, vol. 30, no. 3, pp. 337–347, 2017.